TEXAS
The University of Texas at Austin

COVID-19 scenario projections for Austin, Texas – August 2021

Spencer J. Fox*, Michael Lachmann*, Anass Bouchnita, Spencer Woody, Remy Pasco, Maureen Johnson-Leon, Tanvi Ingle, Kaitlyn Johnson, Lauren Ancel Meyers

* These authors contributed equally

The University of Texas at Austin
COVID-19 Modeling Consortium

utpandemics@austin.utexas.edu

COVID-19 scenario projections for Austin, Texas — August 2021

The University of Texas COVID-19 Modeling Consortium

Contributors: Spencer J. Fox*, Michael Lachmann*, Anass Bouchnita, Spencer Woody, Remy Pasco, Maureen Johnson-Leon, Tanvi Ingle, Kaitlyn Johnson, Lauren Ancel Meyers

* These authors contributed equally

Contact: utpandemics@austin.utexas.edu

Overview

To support public health decision-making and healthcare planning, we developed a model for the five-county Austin-Round Rock Metropolitan Statistical Area (henceforth *Austin*) that can provide real-time estimates of the prevalence and transmission rate of COVID-19 and project healthcare needs into the future.

The model incorporates key epidemiological characteristics of the disease, demographic information for Austin, local vaccination estimates, and local mobility data from anonymized cell phone traces. It uses daily COVID-19 hospitalization data to estimate the changing transmission rate and prevalence of the disease.

In this report, we use COVID-19 hospitalization data for Austin from March 13, 2020 to July 28, 2021 to estimate the state of the pandemic in the summer of 2021 and project hospitalizations through November of 2021. We consider the combined impact of the following factors:

- The emergence of the Delta variant (B.1.617.2), which is estimated to be more highly transmissible and more severe compared to previously circulating variants [1,2].
- The ongoing rollout of SARS-CoV-2 vaccines [3].
- The start of the 2021-2022 school year.
- Various levels of social distancing and facemask usage across Austin and within schools [4]

The projections are based on multiple assumptions about the age-specific severity of COVID-19 and the role of asymptomatic infections in the transmission of the virus. The graphs below do not present the full range of uncertainty for the city of Austin, but are

intended to provide basic insight into the changing risks of COVID-19 transmission, potential healthcare surges, and the impact of facemask and other mitigation guidelines in Austin.

If the Delta variant continues to spread and vaccine uptake continues at the current pace (reaching ~63% of Austin vaccinated with at least one dose by November 1, 2021), then we project that COVID-19 hospitalizations will continue to increase exponentially, threatening healthcare capacity in the region, unless measures are taken to slow transmission. We consider three scenarios in which facemask guidelines and other precautionary measures slow transmission within the community beginning on July 29, 2021 and three scenarios in which facemask guidelines for schools slow transmission among children beginning when schools reopen on August 23, 2021.

We project the following for the three-month period from July 29 to November 1, 2021:

- If community mitigation efforts do not slow transmission, there is a 94% chance that Austin reaches the metropolitan region's ICU capacity of 200 beds by November 1, with a 92% chance of reaching capacity by the end of August. Moderate or high compliance with precautionary recommendations would be expected to reduce the risk of reaching ICU capacity by November 1 to 55% or 36%, respectively.

- If community mitigation efforts do not slow transmission, a school of 100 in-person students would have a 94% chance that at least one of those students would arrive infected on the first day of school (August 23). Moderate or high compliance with precautionary recommendations would be expected to reduce this risk to 54% or 37%, respectively.

- In-person schooling is projected to increase transmission among children and throughout the community. Mask wearing and other precautionary measures within schools would be expected to mitigate some of the additional risk and prevent 36%, 60%, or 50% of pediatric hospitalizations under the low, moderate and high community compliance scenarios.

We are posting these results prior to peer review to provide intuition for both policy makers and the public regarding both the immediate threat of COVID-19. The projections demonstrate the immediate need for heightened social distancing and transmission reducing-precautions within schools and throughout Austin, including keeping physical distance from others, wearing facemasks and self-isolating when symptomatic, alongside an aggressive SARS-CoV-2 vaccination campaign.

Austin COVID-19 transmission model

The appendix describes the model in detail. We use mathematical equations to project the changing numbers of individuals who are susceptible, infected, hospitalized, recovered, deceased, and vaccinated. The model incorporates key features of the virus and vaccination rates by age group in the Austin MSA [3]. The daily transmission rate is estimated using iterated filtering [5] from a combination of local hospital and cell-phone mobility data [6]. The projections below make the following assumptions:

- Epidemic seeding: February 17, 2020 with 1 infected adult
- Transmission rates are modulated by age-specific contact patterns, with contacts among children elevated during the school year [7].
- Following infection, cases go through multiple stages of infection:

  Stage 1: Pre-symptomatic and non-contagious for an average of 2.9 days

  Stage 2: Pre-symptomatic contagious for an average of 2.3 days

  Stage 3: Symptomatic or asymptomatic contagious for an average of 4 days (43% of infections remain asymptomatic and have 33% lower infectiousness than symptomatic cases)
- Cases may be hospitalized or die at rates that depend on age and risk group. For unvaccinated cases infected by non-Delta variants:
  - The overall infection hospitalization rate (IHR) is 4.2% [1]
  - The overall infection fatality rate (IFR) is 0.54% [8]
- The length of hospital stays is estimated from the local data and changes through time.
- Vaccines lower the risk of infection by 80% starting two weeks after receiving a first dose and by 96% starting two weeks after receiving a second dose [9].
- The Delta variant is 64% more transmissible and increases hospitalization risk by 80% relative to prior variants [1,2]. Delta variant decreases vaccine efficacy at preventing infection by 6% (Bernal et al. 2021). We estimate that Delta became the dominant variant in Texas by June 21, 2021, and comprised approximately 93% (95% CI: 92-94%) of infections as of July 28 [10,11].

COVID-19 in Austin through July 28, 2021

Our Austin COVID-19 healthcare forecasting dashboard [12] provides daily estimates of the effective reproduction number, $R(t)$ (Figure 1). This quantity indicates the contagiousness of the virus at a given point in time and roughly corresponds to the average number of people a typical case will infect. Measures to slow or prevent transmission, such as social distancing and wearing facemasks, can reduce the reproduction number. Immunity acquired either through past infection or vaccination can also reduce the reproduction number. If $R(t)$ is greater than one, then an epidemic will continue to grow; if $R(t)$ is less than one, it will begin to subside. By tracking $R(t)$, we can detect whether policies and individual-level behaviors are having the desired impact and project cases, hospitalizations and deaths into the future.

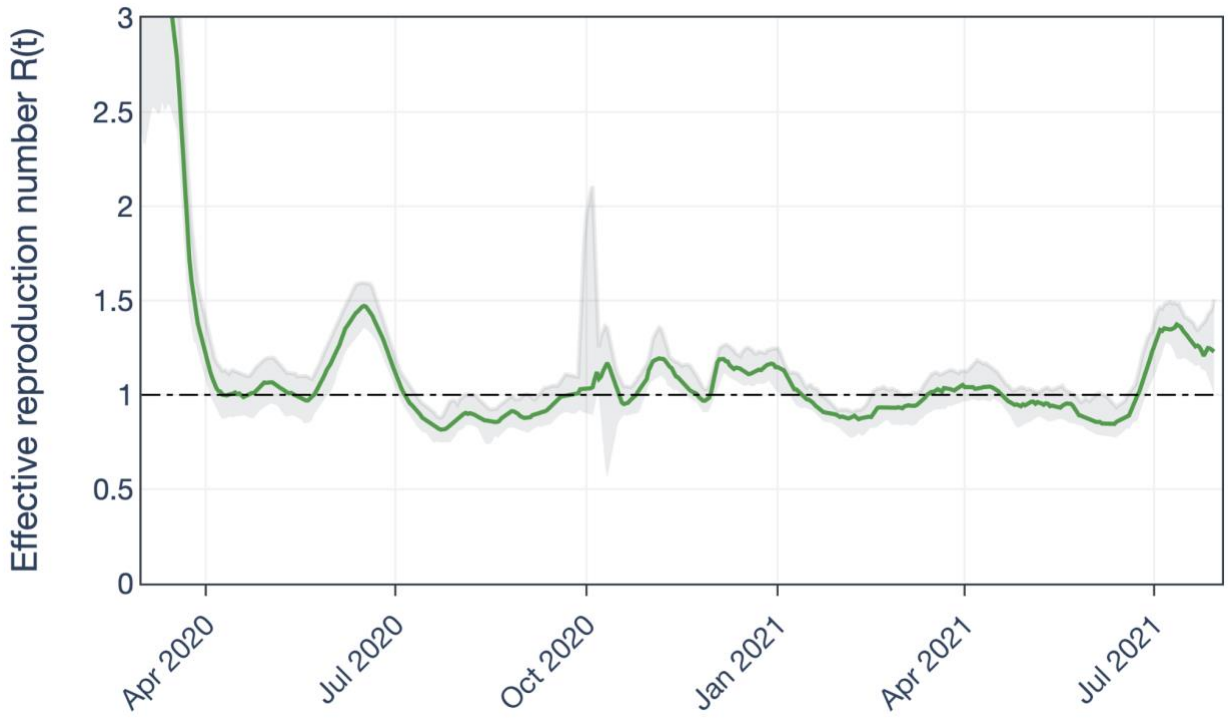

Figure 1: The 7-day average effective reproduction number, *R*(*t*), of the COVID-19 pandemic in Austin from February 17, 2020 to July 28, 2021. $R(t)$ is an epidemiological quantity used to describe the contagiousness of a disease. An epidemic is expected to continue if $R(t)$ is greater than one and to end if $R(t)$ is less than one. This *epidemic threshold* of $R(t) = 1$ is indicated by a horizontal dashed line. $R(t)$ can be interpreted as the average number of people that an infected case will infect. The value of $R(t)$ depends on the basic infectiousness of the disease, the number of people that are susceptible to infection, and the impact of social distancing, mask wearing and other measures to slow transmission. The solid line gives the mean daily estimate and the shaded ribbon indicates the 95% credible interval.

COVID-19 projections under nine community and school mitigation scenarios

The reopening of schools on August 23, 2021 is expected to amplify transmission. Face mask usage and precautionary measures within schools can mitigate some of the risk. We project COVID-19 spread and hospitalizations among adults and children under nine scenarios, in which community mitigation is low, medium or high and in-school mitigation is either low, medium, or high.

Community mitigation scenarios:

- **Status quo**: A reproduction number of 1.2 (95% CrI: 1.0-1.5) estimated on July 28, 2021 does not change. Vaccinations continue to be administered at the rate reported from June 16 to July 1 (840 doses per day), resulting in ~64% of the Austin area population having received at least one dose by November 1, 2021.
- **High compliance scenario:** The reproduction number is reduced by 45%, according to an estimate in Germany following the implementation of mask mandates [4].
- **Moderate compliance scenario:** Compliance is reduced by 25% relative to the high compliance scenario.

School mitigation scenarios:

- **No reopening**: In-person schooling does not occur during the projection period.
- **Schools reopen without mitigation**: On August 23, schools reopen with high in-person attendance and low levels of face mask usage and other precautionary measures.
- **Schools reopen with mitigation**: On August 23, schools reopen with high in-person attendance and high compliance with face masking and other precautionary measures which reduce in-school transmission by 45% [4].

For each scenario, we project COVID-19 hospitalizations, ICU needs, and in-hospital mortality up to November 1, assuming that no other policy or behavioral changes impact the COVID-19 transmission rate during this period (Figures 2-4, Table 1). We also estimate the probability that at least one student in a school with 100 in-person students will arrive at school infected based on projected pediatric infection estimates and the percent of pediatric hospitalizations that can be prevented through mask wearing in schools (Figure 5).

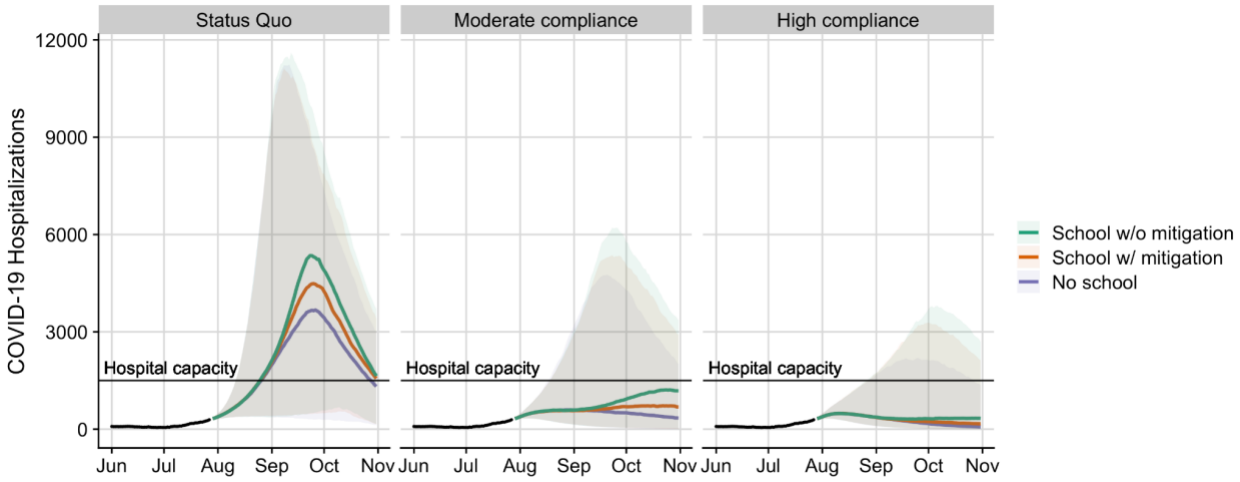

Figure 2: Projected COVID-19 hospitalizations in the Austin-Round Rock MSA from July 29 to November 1, 2021, under the status quo (left graph), moderate compliance (middle graph) and high compliance (right graph) community mitigation scenarios. Black points represent the reported daily COVID-19 patients in all Austin area hospitals. Colored lines represent median projections across 500 stochastic simulations for the three school mitigation scenarios, with shading indicating the 95% prediction intervals. The horizontal black lines indicate the estimated COVID-19 hospital capacity of 1,500 patients in the MSA.

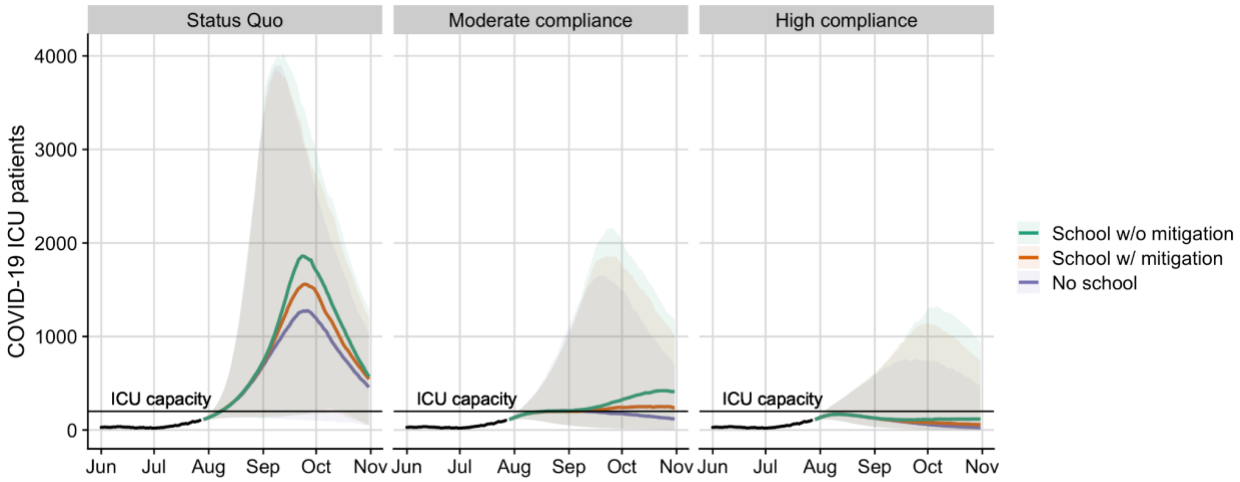

Figure 3: Projected COVID-19 ICU patients in the Austin-Round Rock MSA from July 29 to November 1, 2021, under the status quo (left graph), moderate compliance (middle graph) and high compliance (right graph) community mitigation scenarios. Black points represent the reported daily COVID-19 ICU patients in all Austin area hospitals. Colored lines represent median projections across 500 stochastic simulations for the three school mitigation scenarios, with shading indicating the 95% prediction intervals. The horizontal black lines indicate the estimated ICU capacity of 200 COVID-19 patients in the MSA.

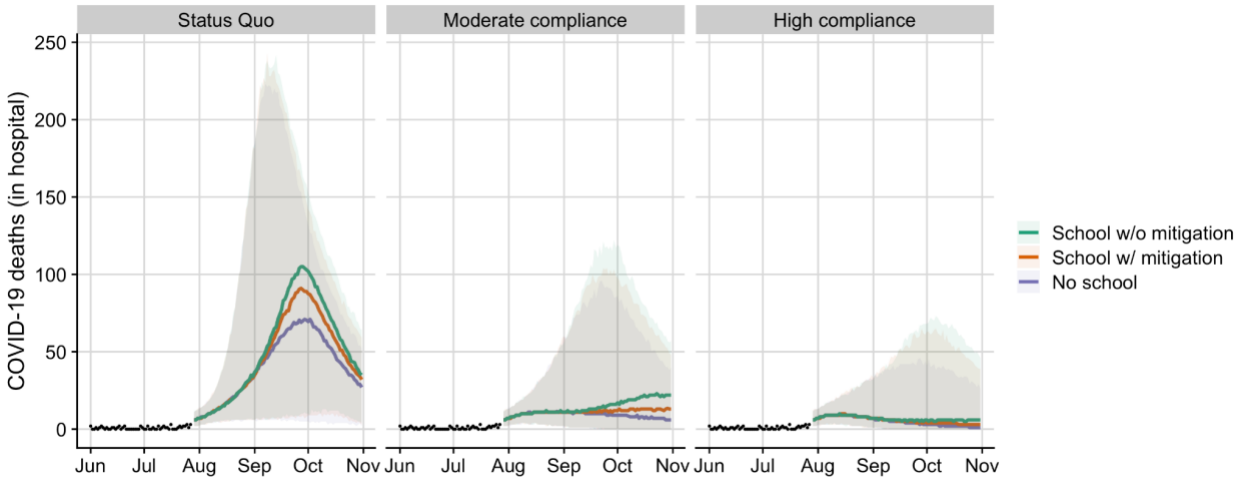

Figure 4: Projected daily COVID-19 in-hospital mortality in the Austin-Round Rock MSA from July 29 to November 1, 2021, under the status quo (left graph), moderate compliance (middle graph) and high compliance (right graph) community mitigation scenarios. Black points represent the daily number of COVID-19 deaths reported by all Austin area hospitals. COVID-19 deaths occurring outside of hospitals are not included in these projections. Colored lines represent median projections across 500 stochastic simulations for the three school mitigation scenarios, with shading indicating the 95% prediction intervals.

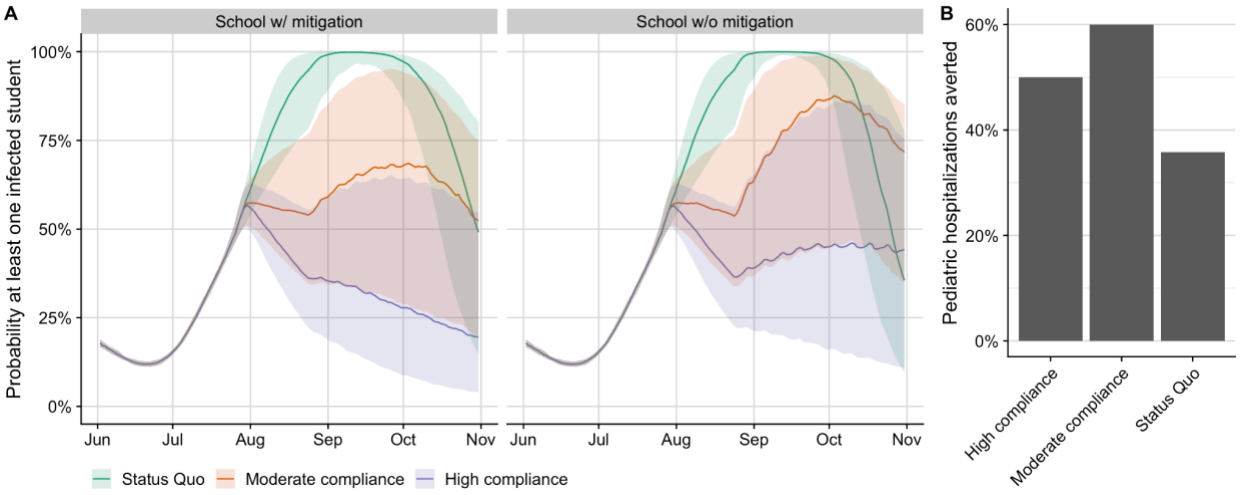

Figure 5: Projected COVID-19 risks to children in the Austin-Round Rock MSA from July 29 to November 1, 2021. (A) Probability that at least one student arrives infected at a school with 100 in-person students. The left graph corresponds to the school reopening scenario in which students wear face masks and adopt cautionary behavior. The right graph corresponds to the school reopening scenario without such mitigation behavior. Line colors correspond to the median projections for the three community mitigation scenarios for Austin. The shaded regions are 50% prediction intervals. (B) The median estimated proportion of pediatric COVID-19 hospitalizations that would be averted through in-school face masking and precautionary behavior between July 29 and November 1, 2021. The x-axis indicates the three different community mitigation scenarios.

Table 1: Projected impact of community and in-school compliance with mitigation efforts on healthcare demand in the Austin-Round Rock MSA from July 29 to November 1, 2021. Numbers are median values with 95% prediction intervals in parenthesis.

Austin Trend	School mitigation	COVID-19 hospitalizations	COVID-19 deaths	Peak ICU usage	Probability of exceeding ICU capacity	Estimated date of reaching ICU capacity*	Probability at least one infected student at school of size 100 on August 23
Status Quo	No school	27,900 (3,800 - 49,500)	4,210 (610-8,490)	1,330 (140-4,050)	94%	Aug 8 (Aug 6-NR)	94% (77%-99%)
	School w/o mitigation	35,200 (7,300 - 51,400)	5,390 (960-8,810)	2,060 (330-4,210)	99%	Aug 8 (Aug 6-Sep 30)	94% (77%-99%)
	School w/ mitigation	32,600 (5,900 - 50,900)	4,990 (870-8,720)	1,700 (215-4,020)	98%	Aug 8 (Aug 6- Oct 12)	94% (77%-99%)
Moderate compliance	No school	5,800 (1,300 - 32,200)	900 (250-5,030)	220 (120-1,700)	55%	Aug 18 (Aug 6-NR)	55% (35%-76%)
	School w/o mitigation	9,900 (1,400 - 37,500)	1,360 (260-5,910)	450 (123-2,270)	69%	Aug 17 (Aug 6-NR)	54% (35%-76%)
	School w/ mitigation	7,400 (1,400 - 35,100)	1,090 (260-5,420)	270 (120-1,920)	59%	Aug 19 (Aug 6-NR)	54% (35%-76%)
High compliance	No school	2,900 (1,000 - 19,300)	490 (200-2,890)	170 (110-770)	36%	NR (Aug 6- NR)	37% (23%-56%)
	School w/o mitigation	4,100 (1,000 - 26,500)	630 (205-3,825)	180 (110-1,390)	44%	NR (Aug 6- NR)	37% (23%-56%)
	School w/ mitigation	3,400 (1,000 - 25,000)	560 (210-3,910)	170 (120-1,160)	39%	NR (Aug 6- NR)	37% (23%-56%)

* *NR* indicates that the projection did not reach the trigger or ICU capacity by November 1.

Appendix

COVID-19 Epidemic Model Structure and Parameters

The model structure is diagrammed in Figure A1 and described in the equations below.
For each age and risk group, we build a separate set of compartments to model the transitions between the states: susceptible (S), exposed (E), pre-symptomatic infectious (P^Y), pre-asymptomatic infectious (P^A), symptomatic infectious (I^Y), asymptomatic infectious (I^A), symptomatic infectious that are hospitalized (I^H), recovered (R), and deceased (D). The symbols S, V, E, E^V, P^Y, P^A ,I^Y, I^A, I^H, R, and D denote the number of people in that state in the given age/risk group and the total size of the age/risk group is

$$N = S + V + E + E^V + P^Y + P^A + I^Y + I^A + I^H + R + D.$$

The deterministic model for individuals in age group a and risk group r is given by:

$$\frac{dS_{a,r}}{dt} = -S_{a,r} \cdot \sum_{i \in A, j \in K} (I^Y_{i,j}\omega^Y + I^A_{i,j}\omega^A + P^Y_{i,j}\omega^{PY} + P^A_{i,j}\omega^{PA})\beta(t)\delta(t)\phi_{a,i}/N_i$$

$$\frac{dE_{a,r}}{dt} = S_{a,r} \cdot \sum_{i \in A, j \in K} (I^Y_{i,j}\omega^Y + I^A_{i,j}\omega^A + P^Y_{i,j}\omega^{PY} + P^A_{i,j}\omega^{PA})\beta(t)\delta(t)\phi_{a,i}/N_i - \sigma E_{a,r}$$

$$\frac{dV_{a,r}}{dt} = v^S_{a,r} - S_{a,r} \cdot \sum_{i \in A, j \in K} (I^Y_{i,j}\omega^Y + I^A_{i,j}\omega^A + P^Y_{i,j}\omega^{PY} + P^A_{i,j}\omega^{PA})\beta(t)\delta_V(t)\phi_{a,i}/N_i$$

$$\frac{dE^V_{a,r}}{dt} = S_{a,r} \cdot \sum_{i \in A, j \in K} (I^Y_{i,j}\omega^Y + I^A_{i,j}\omega^A + P^Y_{i,j}\omega^{PY} + P^A_{i,j}\omega^{PA})\beta(t)\delta_V(t)\phi_{a,i}/N_i - \sigma E^V_{a,r}$$

$$\frac{dP^A_{a,r}}{dt} = (1-\tau)\sigma E_{a,r} + (1-\tau_V)\sigma E^V_{a,r} - \rho^A P^A_{a,r}$$

$$\frac{dP^Y_{a,r}}{dt} = \tau\sigma E_{a,r} + \tau_V \sigma E^V_{a,r} - \rho^Y P^Y_{a,r}$$

$$\frac{dI^A_{a,r}}{dt} = \rho^A P^A_{a,r} - \gamma^A I^A_{a,r}$$

$$\frac{dI^Y_{a,r}}{dt} = \rho^Y P^Y_{a,r} - (1-\pi)\gamma^Y I^Y_{a,r} - \pi\eta\delta_H(t) I^Y_{a,r}$$

$$\frac{dI^H_{a,r}}{dt} = \pi\eta\delta_H(t) I^Y_{a,r} - (1-\nu)\gamma^H(t) I^H_{a,r} - \nu\mu(t) I^H_{a,r}$$

$$\frac{dR_{a,r}}{dt} = \gamma^A I^A_{a,r} + (1-\pi)\gamma^Y I^Y_{a,r} + (1-\nu)\gamma^H(t) I^H_{a,r}$$

$$\frac{dD_{a,r}}{dt} = \nu\mu(t) I^H_{a,r}$$

where A and K are all possible age and risk groups, ω^A , $\omega^Y, \omega^{PA}, \omega^{PY}$ are the relative infectiousness of the I^A , I^Y, I^{PA}, I^{PY} compartments, respectively, β is transmission rate, $\phi_{a,i}$ is the mixing rate between age group $a, i \in A$, and $\gamma^A, \gamma^Y, \gamma^H(t)$ are the recovery rates for the I^A , I^Y, I^H compartments, respectively, σ is the exposed rate, ρ^A, ρ^Y are the pre-(a)symptomatic rates, τ is the symptomatic ratio, π is the proportion of symptomatic individuals requiring hospitalization, η is rate at which hospitalized cases enter the hospital following symptom onset, ν is mortality rate for hospitalized cases, $\mu(t)$ is daily instantaneous rate at which terminal patients die, $v^S_{a,r}$ is the estimated number of susceptible individuals who are vaccinated on a given day as described below, $\delta(t)$ is the increase of chance of infection due to Delta variant, $\delta_V(t)$ is the increase of chance of infection of vaccinated individuals due to Delta variant, and δ_H is the increased chance of hospitalization due to the Delta variant.

We simulate the model using a stochastic implementation of the deterministic equations. Transitions between compartments are governed using the τ-leap method [13,14] with key parameters given in Table A1-2. We simulate the model according to the following equations:

$$
\begin{gathered}
S_{a,r}(t+1) - S_{a,r}(t) = -P_1 - P_{10} \\
E_{a,r}(t+1) - E_{a,r}(t) = P_1 - P_2 \\
E^V_{a,r}(t+1) - E^V_{a,r}(t) = P'_1 - P'_2 \\
P^A_{a,r}(t+1) - P^A_{a,r}(t) = (1-\tau)P_2 + (1-\tau_V)P'_2 - P_3 \\
P^Y_{a,r}(t+1) - P^Y_{a,r}(t) = \tau P_2 + \tau_V P'_2 - P_4 \\
I^A_{a,r}(t+1) - I^A_{a,r}(t) = P_3 - P_5 \\
I^Y_{a,r}(t+1) - I^Y_{a,r}(t) = P_4 - P_6 - P_7 \\
I^H_{a,r}(t+1) - I^H_{a,r}(t) = P_7 - P_8 - P_9 \\
R_{a,r}(t+1) - R_{a,r}(t) = P_5 + P_6 + P_8 \\
V_{a,r}(t+1) - V_{a,r}(t) = P_{10} - P'_1
\end{gathered}
$$

with

$$
\begin{gathered}
P_1 \sim B(n = S_{a,r}(t),\, p = 1 - e^{-(F_{a,r}(t))\cdot dt}) \\
P'_1 \sim B(n = S_{a,r}(t),\, p = 1 - e^{-(F^V_{a,r}(t))\cdot dt}) \\
P_2 \sim B(n = E_{a,r}(t),\, p = 1 - e^{-(\sigma)\cdot dt}) \\
P'_2 \sim B(n = E^V_{a,r}(t),\, p = 1 - e^{-(\sigma)\cdot dt}) \\
P_3 \sim B(n = P^A_{a,r}(t),\, p = 1 - e^{-(\rho^A)\cdot dt}) \\
P_4 \sim B(n = P^Y_{a,r}(t),\, p = 1 - e^{-(\rho^Y)\cdot dt}) \\
P_5 \sim B(n = I^A_{a,r}(t),\, p = 1 - e^{-(\gamma^A)\cdot dt}) \\
P_6 \sim B(n = I^Y_{a,r}(t),\, p = 1 - e^{-((1-\pi)\gamma^Y)\cdot dt}) \\
P_7 \sim B(n = I^Y_{a,r}(t),\, p = 1 - e^{-(\pi\eta\delta_H(t))\cdot dt}) \\
P_8 \sim B(n = I^H_a,\, p = 1 - e^{-((1-\nu)\gamma^H(t))\cdot dt}) \\
P_9 \sim B(n = I^H_{a,r}(t),\, p = 1 - e^{-(\nu\mu(t))\cdot dt})
\end{gathered}
$$

where *B*(*n*,*p*) denotes a binomial distribution with *n* trials each with probability of success *p*. Transitions from S to V as a result of vaccination events happen once a day, dependent on covariate data supplied to the model. The number of doses given on that day to the age and risk group is given as $v_{a,r}$. The number of doses given to individuals who are susceptible is then $v^S_{a,r}$, and of those, those that are effective are $v^{\text{eff}}_{a,r}$, where

$$v^S_{a,r}(t) \sim H(S(t)_{a,r}, N_{a,r} - S_{a,r}, v_{a,r}(t))$$
$$v^{\text{eff}}_{a,r}(t) \sim B(v^S_{a,r}(t), \epsilon_V)$$

So that

$$P_{10} \sim B(H(S(t)_{a,r}, N_{a,r} - S_{a,r}, v_{a,r}(t)), \epsilon_V)$$

With $H(N_1, N_2, n)$ defining the hyper-geometric distribution.

$F_{a,r}$ and $F^V_{a,r}$ denote the force of infection for unvaccinated and vaccinated individuals in age group a and risk group r and is given by

$$F_{a,r}(t) = \sum_{i \in A, j \in K} (I^Y_{i,r}(t)\omega^Y + I^A_{i,r}(t)\omega^A + P^Y_{i,j}(t)\omega^{PY} + P^A_{i,j}(t)\omega^{PA})\beta(t)\delta(t)\phi_{a,i}/N_i$$

$$F^V_{a,r}(t) = \sum_{i \in A, j \in K} (I^Y_{i,r}(t)\omega^Y + I^A_{i,r}(t)\omega^A + P^Y_{i,j}(t)\omega^{PY} + P^A_{i,j}(t)\omega^{PA})\beta(t)\delta_V(t)\phi_{a,i}/N_i$$

with

$$\beta(t) = e^{\log(\beta(0)) + b_1(t)\cdot PC1 + b_2(t)\cdot PC2 + Z(t) + AZ(t)}$$
$$b_1(t) \sim N(b_1(t-1), \sigma_{b_1})$$
$$b_2(t) \sim N(b_2(t-1), \sigma_{b_2})$$
$$Z(t) \sim N(0.97 \cdot Z(t-1), \sigma_Z), Z(0) = 0.$$

where PC1 and PC2 describe the first and second principal components from our mobility data as described below. The adjustment $AZ(t)$ modifies $\beta(t)$ to model the impacts of increased mask wearing:

$$AZ(t) = A_m(t)$$

where $A_m(t)$ indicates the impact of masking,

Finally,

$\mu(t) = e^{\log(\mu(0)) + Z_\mu}$ where $Z_\mu(t) \sim N(\psi_\mu \cdot Z_\mu(t-1), \sigma_\mu)$, $Z_\mu(0) = 0$ and
$\gamma^H(t) = e^{\log(\gamma^H(0)) + Z_\gamma}$ where $Z_\gamma(t) \sim N(0.99 \cdot Z_\gamma(t-1), \sigma_\gamma)$, $Z\gamma(0) = 0$.

We estimate $\beta(t)$, k, σ_Z, $b_1(t)$, $b_2(t)$, σ_{b_1}, σ_{b_2}, ψ_μ, σ_μ, and σ_γ as described in the model fitting section below.

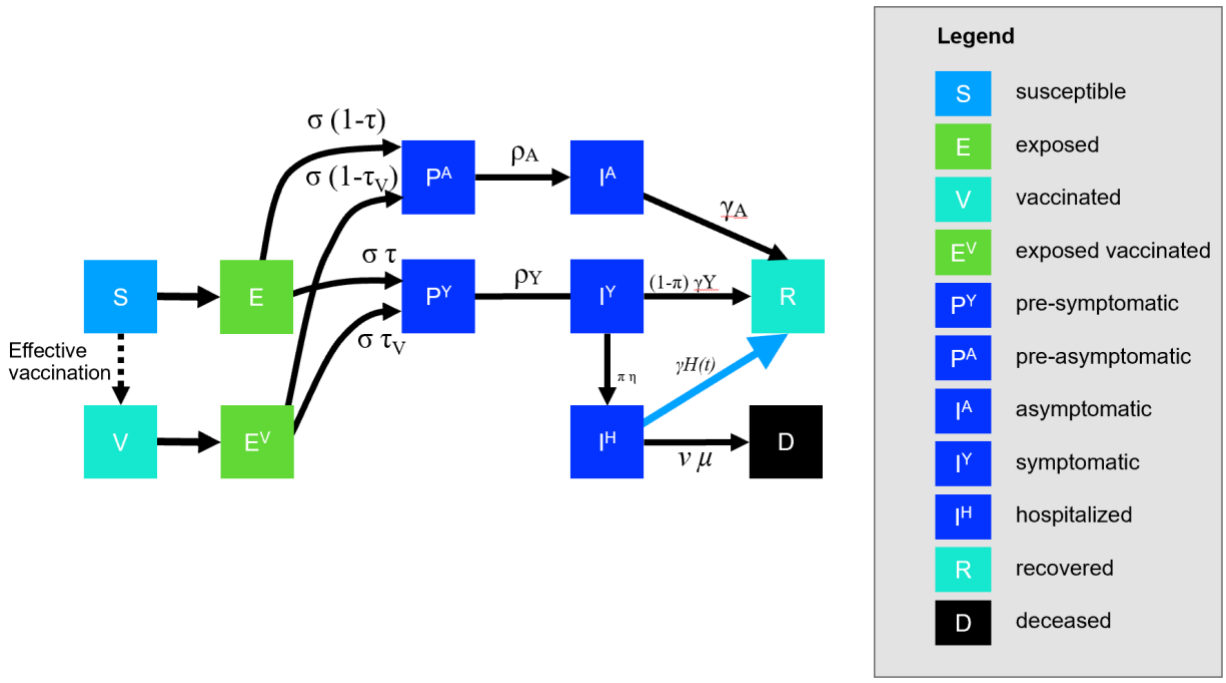

Figure A1. Compartmental model of COVID-19 transmission in the Austin MSA. Each subgroup (defined by age and risk) is modeled with a separate set of compartments. Upon infection, susceptible individuals (*S*) progress to exposed (*E*) or vaccinated (V). Exposed individuals progress to either pre-symptomatic infectious (P^Y) or pre-asymptomatic infectious (P^A) from which they move to symptomatic infectious (I^Y) and asymptomatic infectious (I^A), respectively. All asymptomatic cases eventually progress to a recovered class where they remain protected from future infection (*R*); symptomatic cases are either hospitalized (I^H) or recover. Mortality (*D*) varies by age group and risk group and is assumed to be preceded by hospitalization. Vaccinated individuals can also become exposed to the virus when the Delta variant is circulating and are moved to the E^V compartment when infected.

Projecting vaccination rates by age and risk group

We project future vaccination rates based on past vaccination trends in the Austin-Round Rock, TX MSA according to data from the Texas Department of State Health Services (DSHS) [3]. DSHS provides data online on vaccinations across Texas by county and age group. We aggregate age groups across the five county MSA to obtain estimates for the number of doses that have been distributed within the MSA for each age group. DSHS provides vaccination data according to four age groups, and we convert these numbers to our model age groups proportionate to the respective populations. We project vaccinations forward after July 16 assuming that vaccination trends from the previous four weeks continue into the future, meaning that we take the average number of daily doses delivered from this time period and project forward. Though we do not have vaccination data by risk group, we assume vaccines are allocated to high-risk groups within each age group first until they reach 90% coverage, and then allocate vaccines to the low-risk group.

Projecting Delta variant prevalence

To project prevalence of the Delta SARS-CoV-2 variant, we use time series sequencing data for Texas from the online genomic surveillance data repository GISAID.org (Figure A2). We fit a Bayesian logistic regression model to these data to estimate the relative growth rate of Delta against all other existing SARS-CoV-2 variants [15] . With these data, we estimate the Delta has a logistic growth rate of 0.076 (95% CI: 0.072-0.080), corresponding to an early doubling time of 13.1 days (95% CI: 12.6-13.7 days). This is slightly lower than the relative growth rate observed in Great Britain, which was approximately 0.111 with a doubling time of 9.0 days, which could be due to the competing presence of the gamma variant (P.1) in the United States.

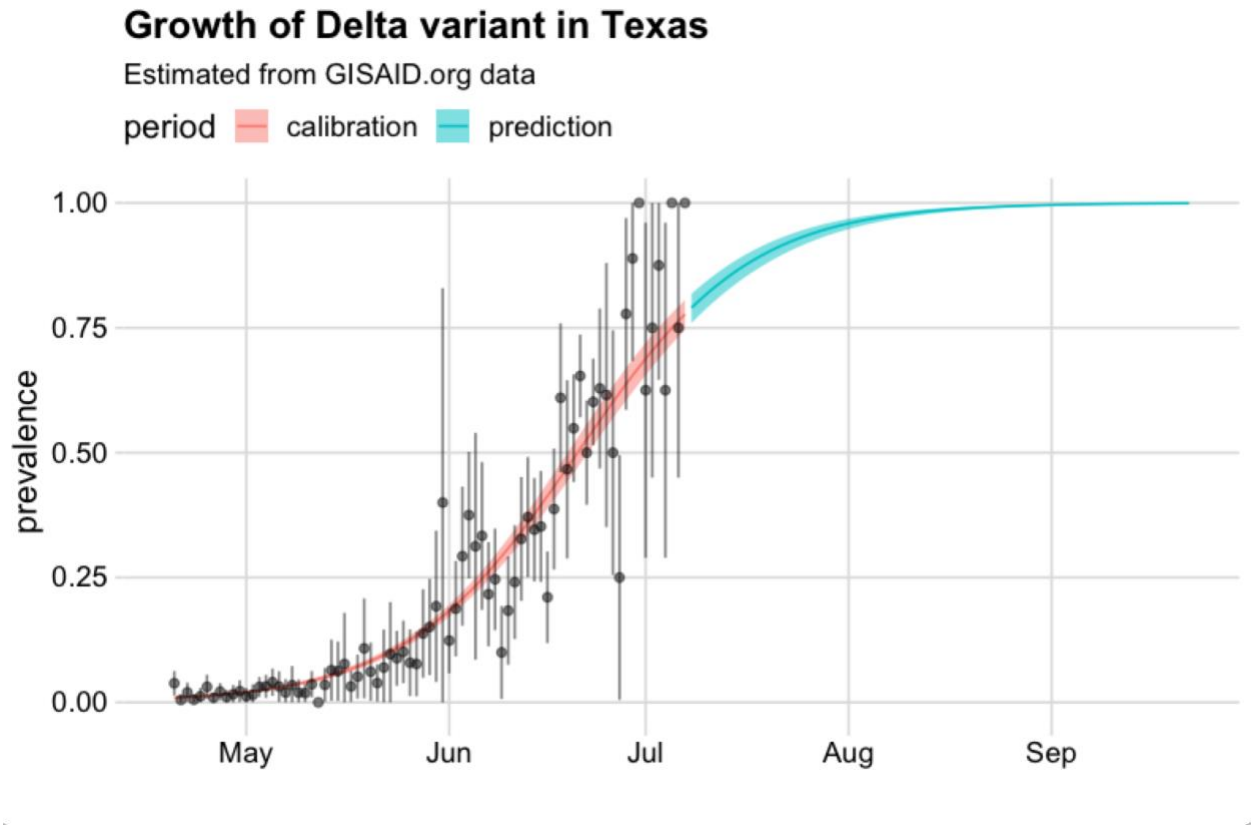

Figure A2: Daily prevalence of Delta variant among all SARS-CoV-2 infections, according to GISAID.org data. Points represent daily prevalence of the variant among all sequences, with bars representing 95% confidence intervals. We fit a Bayesian logistic regression model to the data to smooth over daily variation and project Delta prevalence through October 1, 2021. We estimate that Delta became the dominant variant in Texas by June 21, 2021, and comprised approximately 93% (95% CI: 92-94%) of infections as of July 28 [10,11].

Impact of Delta on Healthcare Projections

In the main text, we assume that Delta increases the likelihood of infected individuals needing to be hospitalized, but this is a key uncertain parameter for scenario projections. Here we show similar projections if Delta does not impact the severity of infections (Figure A3-A5).

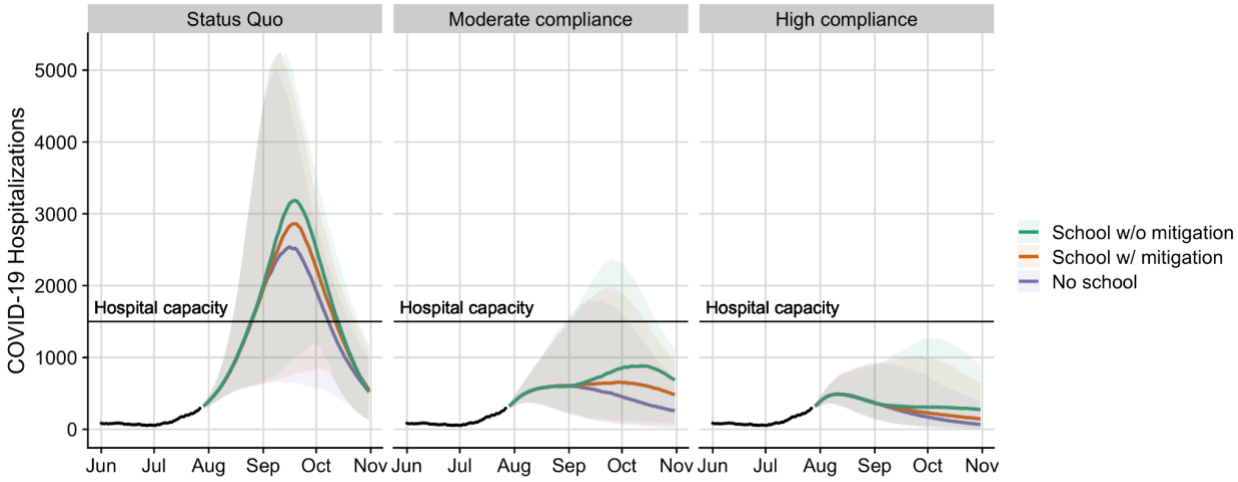

Figure A3: Projected COVID-19 hospitalizations in the Austin-Round Rock MSA from July 29 to November 1, 2021. Black points represent the reported daily COVID-19 patients in all Austin area hospitals. Colored lines represent median projections across 500 stochastic simulations for the school masking scenarios, with colored ribbons representing the 95% prediction interval. Columns indicate community transmission scenarios. The horizontal black line indicates the estimated COVID-19 hospital capacity of 1,500 patients in the MSA.

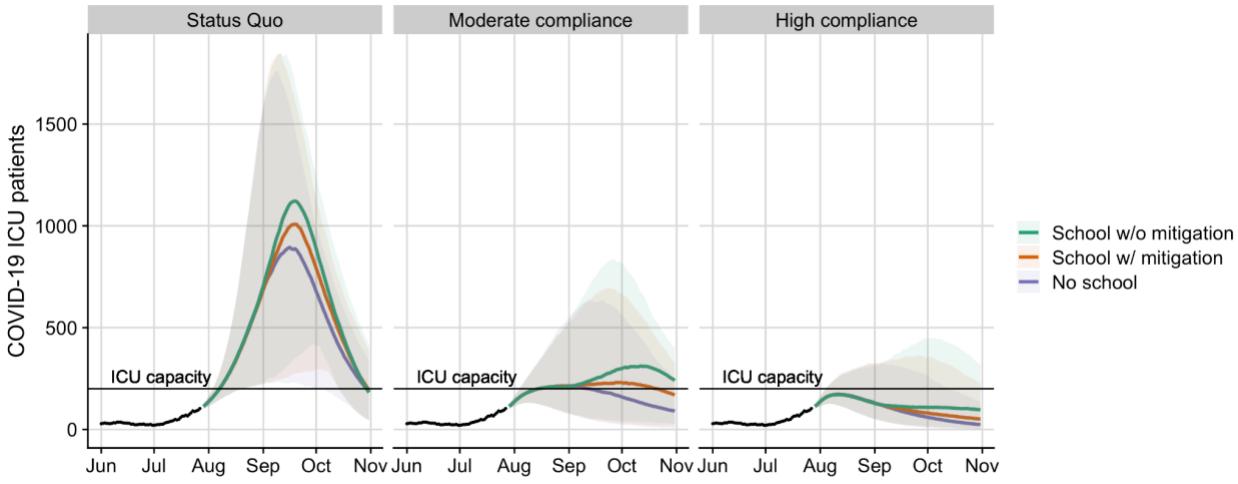

Figure A4: Projected COVID-19 ICU patients in the Austin-Round Rock MSA from July 29 to November 1, 2021. Black points represent the reported daily COVID-19 ICU patients in all Austin area hospitals. Colored lines represent median projections across 500 stochastic simulations for the school masking scenarios, with colored ribbons representing the 95% prediction interval. Columns indicate community transmission scenarios. The horizontal black line indicates the estimated ICU capacity of 200 COVID-19 patients in the MSA.

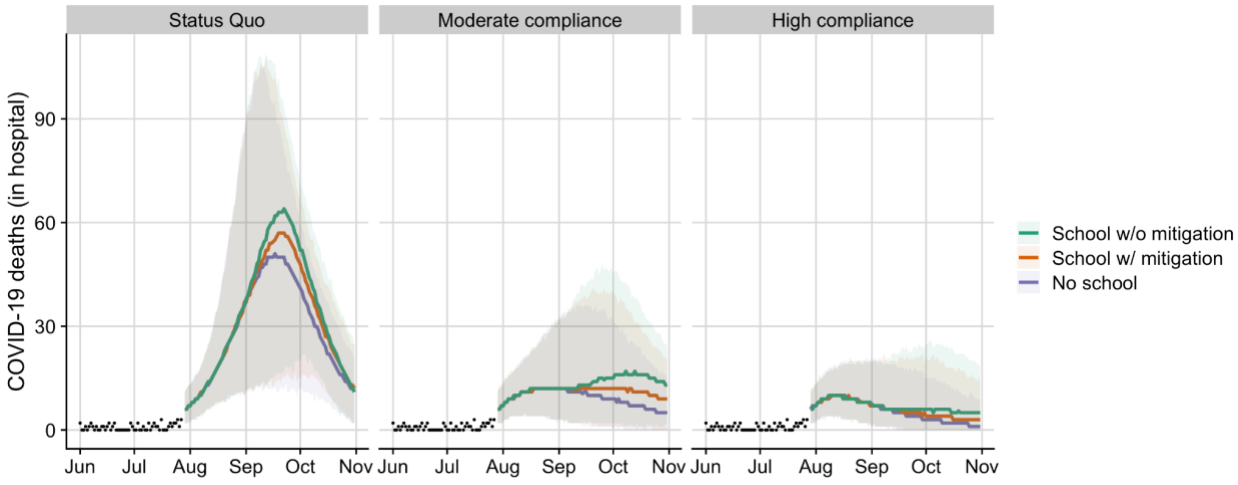

Figure A5: Projected COVID-19 in-hospital mortality in the Austin-Round Rock MSA from July 29 to November 1, 2021. Black points represent the daily number of COVID-19 deaths reported by all Austin area hospitals. COVID-19 deaths occurring outside of hospitals are not included in these projections. Colored lines represent median projections across 500 stochastic simulations for the school masking scenarios, with colored ribbons representing the 95% prediction interval. Columns indicate community transmission scenarios.

Mobility trends

We used mobility trends data from the Austin MSA to inform the transmission rate in our model. Specifically, we ran a principal component analysis (PCA) on seven independent mobility variables provided by SafeGraph, including home dwell time and visits to universities, bars, grocery stores, museums and parks, schools, and restaurants [6]. We regressed the transmission rate on the first two principal components from the mobility data as described in the modeling equations for $\beta(t)$.

Epidemic starting conditions

We could not estimate the epidemic start date directly using our model, because the transmission rate flexibility gave rise to similarly good fits within a wide-range of potential values for t_0. We therefore conducted an independent estimation procedure to obtain reasonable epidemic start dates for Austin. We then used our best guess parameters as described in Table A2 and chose $\beta(0) = 0.67$ as it produced three-day doubling rate in cumulative cases and gave $R_t(0) = 4$ which are consistent with observations for the Austin early outbreak dynamics [16]. We ran 1,000 stochastic simulations with these initial conditions, and identified the wait time for when there was 1 admit for Austin. We estimated the start time from the resulting distribution of wait times for Austin as February 17, 2020 (IQR = February 11 - February 23), and chose February 17th, 2020 as the start date for the model.

Model likelihood

We obtained daily hospital admit ($H_A(t)$), discharge data ($H_L(t)$), total hospitalizations ($H(t)$), and death data ($H_D(t)$) for the Austin MSA. In this model we estimated $\beta(t)$, k, σ_Z, $b_1(t)$, $b_2(t)$, σ_{b_1}, σ_{b_2}, ψ_μ, σ_μ, σ_γ and fixed the remaining parameters as described in Table A1-2. We assumed all sources of data were negative binomially distributed around their predicted values from the SEIR stochastic model, and chose informative, but relatively dispersed priors for certain parameters for stability in parameter estimation and to prevent the model from overfitting data through large perturbations to time-dependent variables.

Following all of these considerations, the likelihood for our stochastic model was:

$$p(Y(t), b_1(0), \sigma_{b_1}, b_2(0), \sigma_{b_2}, k|\theta) = p(Y(t)|\theta, b_1(0), \sigma_{b_1}, b_2(0), \sigma_{b_2}, k) \cdot p(\theta, b_1(0), \sigma_{b_1}, b_2(0), \sigma_{b_2}, k)$$

where $Y(t)$ refers to the four types of data from hospitals, θ contains all parameters from Table A1 not explicitly listed, and where

$$p(Y(t)|\theta, b_1(0), \sigma_{b_1}, b_2(0), \sigma_{b_2}, k) = p(H_A(t)|\hat{H}_A(t))p(H_L(t)|\hat{H}_L(t))p(H_D(t)|\hat{H}_D(t))p(H(t)|\hat{H}(t))$$
$$p(\theta, b_1(0), \sigma_{b_1}, b_2(0), \sigma_{b_2}, k) = p(b_1(0)) \cdot p(\sigma_{b_1}) \cdot p(b_2(0)) \cdot p(\sigma_{b_2}) \cdot p(k)$$

with

$$p(H_A(t)|\hat{H}_A(t)) = \binom{k + H_A(t) - 1}{H_A(t)} \cdot p^k (1-p)^{H_A(t)}, \text{ and } p = \frac{k}{k + \hat{H}_A(t)}$$

$$p(H_L(t)|\hat{H}_L(t)) = \binom{k + H_L(t) - 1}{H_L(t)} \cdot p^k (1-p)^{H_L(t)}, \text{ and } p = \frac{k}{k + \hat{H}_L(t)}$$
$$p(H_D(t)|\hat{H}_D(t)) = \binom{k + H_D(t) - 1}{H_D(t)} \cdot p^k (1-p)^{H_D(t)}, \text{ and } p = \frac{k}{k + \hat{H}_D(t)}$$
$$p(H(t)|\hat{H}(t)) = \binom{k + H(t) - 1}{H(t)} \cdot p^k (1-p)^{H(t)}, \text{ and } p = \frac{k}{k + \hat{H}(t)}$$
$$p(b_1(0)) \cdot t_d = \frac{1}{\sqrt{2}} e^{-\frac{1}{2}(\hat{b}_1(0))^2}$$
$$p(b_2(0)) \cdot t_d = \frac{1}{\sqrt{2}} e^{-\frac{1}{2}(\hat{b}_2(0))^2}$$
$$p(\sigma_{b_1}) \cdot t_d = \frac{1}{\Gamma(1.1) \cdot \frac{1}{1.1}^{1.1}} \hat{\sigma}_{b_1}^{1.1-1} e^{-1.1 \cdot \hat{\sigma}_{b_1}}$$
$$p(\sigma_{b_2}) \cdot t_d = \frac{1}{\Gamma(1.1) \cdot \frac{1}{1.1}^{1.1}} \hat{\sigma}_{b_2}^{1.1-1} e^{-1.1 \cdot \hat{\sigma}_{b_2}}$$
$$p(k) \cdot t_d = e^{\hat{k}}$$

and t_d is the number of days in the fitting time period.

Fitting method

In this model we estimated $\beta(t)$, k, σ_Z, $b_1(t)$, $b_2(t)$, σ_{b_1}, σ_{b_2}, ψ_μ, σ_μ, σ_γ and fixed the remaining parameters as described in Table A1. Fitting was carried out using the iterated filtering algorithm made available through the mif2 function in the pomp package in R [17,18]. This algorithm is a stochastic optimization procedure; it performs maximum likelihood estimation using a particle filter to provide a noisy estimate of the likelihood for a given combination of the parameters. For each parameter combination we ran 1,000 iterations of iterated filtering, each with 10,000 particles. We calculated smoothed posterior estimates for all of the states within the model through time (including $\beta(t)$ and other time-dependent parameters which are technically state variables in our model formulation, as it changes through time according to a stochastic process). We calculated these smoothed posteriors as follows:

1. We ran 1,000 independent particle filters at the MLE, each with 10,000 particles. For each run, l, of particle filtering, we kept track of the complete trajectory of each particle, as well as the filtered estimate of the likelihood, L_l.

2. For each of the 1,000 particle filtering runs, we randomly sampled a single complete particle trajectory, giving us 1,000 separate trajectories for all state variables.

3. We resampled from these trajectories with probabilities proportional to L_l to give a distribution of state trajectories

The result can be thought of as an empirical-Bayes posterior distribution: that is, a set of 1,000 smoothed posterior draws from all state variables, conditional on the maximum likelihood estimates for the model's free parameters. This smoothed posterior distribution is how we calculate means and credible intervals for $\beta(t)$ in addition to all other time-varying state variables.

Table A1. Model parameters[a]

Parameters	Value	Source
Start date	February 17, 2020	Estimated
Initial infections	1 symptomatic case age 18-49y	Assumption
$\beta(t)$: daily transmission rate	N/A	Estimated
γ^A: recovery rate on asymptomatic compartment	Equal to γ^Y	Assumption
γ^Y: recovery rate on symptomatic non-treated compartment	0.25	He et al. [19]
τ: symptomatic proportion	0.57	Fox et al. [20]
τ_V: symptomatic proportion among vaccinated	0.055	[21]
ϵ_V effectiveness of single dose	0.80	[9]
σ: exposed rate	1/2.9	Zhang et al. [22]; He et al. [19]
ρ^A: pre-asymptomatic rate	Equal to ρ^Y	
ρ^Y: pre-symptomatic rate	$\frac{1}{2.3}$	He et al. [19]
P: proportion of pre-symptomatic transmission	0.44	He et al. [19]
ω^P: relative infectiousness of pre-symptomatic individuals	$\omega^P = \frac{P}{1-P}\frac{\tau\omega^Y[YHR/\eta + (1-YHR)/\gamma^Y] + (1-\tau)\omega^A/\gamma^A}{\tau\omega^Y/\rho^Y + (1-\tau)\omega^A/\rho^A}$ $\omega^{PY} = \omega^P\omega^Y, \omega^{PA} = \omega^P\omega^A$	
ω^A: relative infectiousness of infectious individuals in compartment I^A	$\frac{2}{3}$	He et al. [23]
IFR: infected fatality ratio, age specific (%)	Low risk: [0.0009, 0.0022, 0.0339, 0.2520, 0.6440] High risk: [0.0092, 0.0218, 0.3388, 2.5197, 6.4402]	Age adjusted from Verity et al. [8]
YFR: symptomatic fatality ratio, age specific (%)	Low risk: [0.001608, 0.003823, 0.05943, 0.4420, 1.130] High risk: [0.01608, 0.03823, 0.5943, 4.420, 11.30]	$YFR = \frac{IFR}{\tau}$

h: high-risk proportion, age specific (%)	[8.2825, 14.1121, 16.5298, 32.9912, 47.0568]	Estimated using 2015-2016 Behavioral Risk Factor Surveillance System (BRFSS) data with multilevel regression and poststratification using CDC's list of conditions that may increase the risk of serious complications from influenza [24–26]
$\delta(t)$ increase of chance of infection due to Delta variant	$\delta(t) = (1 - p_\delta) \cdot 1 + (p_\delta) \cdot 1.6$	[1,2]
$\delta_V(t)$ increase of chance of infection of vaccinated individuals due to Delta variant	$\delta_V(t) = (1 - p_\delta) \cdot 0 + (p_\delta) \cdot 0.055$	[21]
$\delta_H(t)$ increase of chance of hospitalization due to Delta variant	$\delta_H(t) = (1 - p_\delta) \cdot 1 + (p_\delta) \cdot 1$ or $\delta_H(t) = (1 - p_\delta) \cdot 1 + (p_\delta) \cdot 1.8$	[1]

[a]Values given as five-element vectors are age-stratified with values corresponding to 0-4, 5-17, 18-49, 50-64, 65+ year age groups, respectively.

Table A2 Hospitalization parameters

Parameters	Value	Source
$\gamma^H(t)$: recovery rate in hospitalized compartment	Fitted	
YHR: symptomatic case hospitalization rate (%)	Low risk: [0.04021, 0.03091, 1.903, 4.114, 4.879] High risk: [0.4021, 0.3091, 19.03, 41.14, 48.79]	Age adjusted from Verity et al. [8]
π: rate of symptomatic individuals go to hospital, age-specific	$\pi = \frac{\gamma^Y * YHR}{\eta + (\gamma^Y - \eta)YHR}$	
η: rate from symptom onset to hospitalized	0.1695	5.9 day average from symptom onset to hospital admission Tindale et al. [27]

$\mu(t)$: rate from hospitalized to death	Fitted	
HFR: hospitalized fatality ratio, age specific (%)	[4, 12.365, 3.122, 10.745, 23.158]	$HFR = \frac{IFR}{\tau}$
ν: death rate on hospitalized individuals, age specific	$\nu = \frac{\gamma^H HFR}{\mu + (\gamma^H - \mu)HFR}$	
ICU: proportion hospitalized people in ICU	0.36	Estimated from Austin COVID-19 hospitalization data

Table A3 Contact matrix. Daily number contacts by age group on an average day.

	0-4y	**5-17y**	**18-49y**	**50-64y**	**65y+**
0-4y	1.88	2.02	4.01	0.79	0.28
5-17y	0.55	7.06	5.02	0.70	0.22
18-49y	0.37	2.19	8.72	1.45	0.21
50-64y	0.33	1.62	5.79	2.79	0.50
65y+	0.19	0.88	2.36	1.19	1.22

Estimation of age-stratified proportion of population at high-risk for COVID-19 complications

We estimate age-specific proportions of the population at high risk of complications from COVID-19 based on data for Austin, TX and Round-Rock, TX from the CDC's 500 cities project (Figure A6) [28]. We assume that high risk conditions for COVID-19 are the same as those specified for influenza by the CDC [24]. The CDC's 500 cities project provides city-specific estimates of prevalence for several of these conditions among adults [29]. The estimates were obtained from the 2015-2016 Behavioral Risk Factor Surveillance System (BRFSS) data using a small-area estimation methodology called multi-level regression and poststratification [25,26]. It links geocoded health surveys to high spatial resolution population demographic and socioeconomic data [26].

Estimating high-risk proportions for adults. To estimate the proportion of adults at high risk for complications, we use the CDC's 500 cities data, as well as data on the prevalence of HIV/AIDS, obesity and pregnancy among adults (Table A6).

The CDC 500 cities dataset includes the prevalence of each condition on its own, rather than the prevalence of multiple conditions (e.g., dyads or triads). Thus, we use separate co-morbidity estimates to determine overlap. Reference about chronic conditions [30] gives US estimates for the proportion of the adult population with 0, 1 or 2+ chronic conditions, per age group. Using this and the 500 cities data we can estimate the proportion of the population p_{HR} in each age group in each city with at least one chronic condition listed in the CDC 500 cities data (Table A6) putting them at high-risk for flu complications.

HIV: We use the data from table 20a in CDC HIV surveillance report [31] to estimate the population in each risk group living with HIV in the US (last column, 2015 data). Assuming independence between HIV and other chronic conditions, we increase the proportion of the population at high-risk for influenza to account for individuals with HIV but no other underlying conditions.

Morbid obesity: A BMI over 40kg/m^2 indicates morbid obesity, and is considered high risk for influenza. The 500 Cities Project reports the prevalence of obese people in each city with BMI over 30kg/m^2 (not necessarily morbid obesity). We use the data from table 1 in Sturm and Hattori [32] to estimate the proportion of people with BMI>30 that actually have BMI>40 (across the US); we then apply this to the 500 Cities obesity data to estimate the proportion of people who are morbidly obese in each city. Table 1 of Morgan et al. [33] suggests that 51.2% of morbidly obese adults have at least one other high risk chronic condition, and update our high-risk population estimates accordingly to account for overlap.

Pregnancy: We separately estimate the number of pregnant women in each age group and each city, following the methodology in CDC reproductive health report [34]. We assume independence between any of the high-risk factors and pregnancy, and further assume that half the population are women.

Estimating high-risk proportions for children. Since the 500 Cities Project only reports data for adults 18 years and older, we take a different approach to estimating the proportion of children at high risk for severe influenza. The two most prevalent risk factors for children are asthma and obesity; we also account for childhood diabetes, HIV and cancer.
From Miller et al. [35], we obtain national estimates of chronic conditions in children. For asthma, we assume that variation among cities will be similar for children and adults. Thus, we use the relative prevalences of asthma in adults to scale our estimates for children in each city. The prevalence of HIV and cancer in children are taken from CDC HIV surveillance report [31] and cancer research report [36], respectively.

We first estimate the proportion of children having either asthma, diabetes, cancer or HIV (assuming no overlap in these conditions). We estimate city-level morbid obesity in children using the estimated morbid obesity in adults multiplied by a national constant ratio for each age group estimated from Hales et al. [37], this ratio represents the prevalence in morbid obesity in

children given the one observed in adults. From Morgan et al. [33], we estimate that 25% of morbidly obese children have another high-risk condition and adjust our final estimates accordingly.

Resulting estimates. We compare our estimates for the Austin-Round Rock Metropolitan Area to published national-level estimates [38] of the proportion of each age group with underlying high risk conditions (Table A6). The biggest difference is observed in older adults, with Austin having a lower proportion at risk for complications for COVID-19 than the national average; for 25-39 year olds the high risk proportion is slightly higher than the national average.

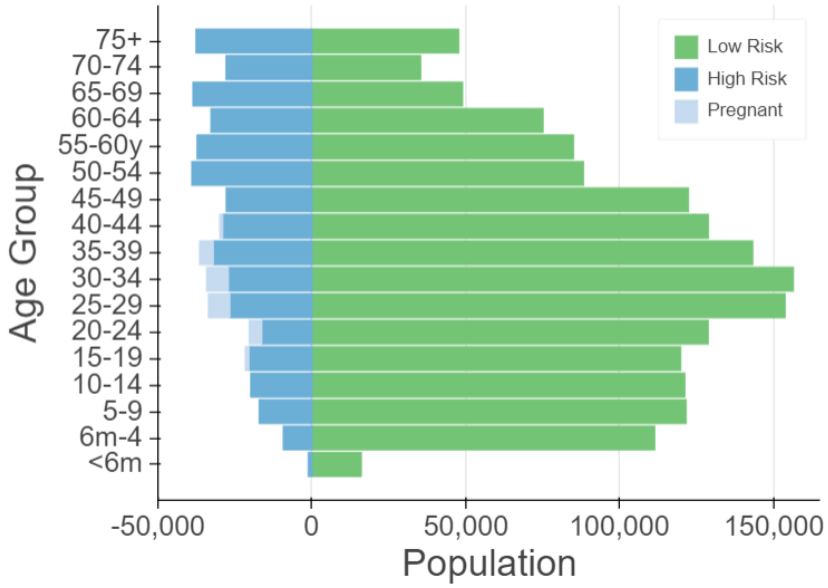

Figure A6. Demographic and risk composition of the Austin-Round Rock MSA. Bars indicate age-specific population sizes, separated by low risk, high risk, and pregnant. High risk is defined as individuals with cancer, chronic kidney disease, COPD, heart disease, stroke, asthma, diabetes, HIV/AIDS, and morbid obesity, as estimated from the CDC 500 Cities Project [28], reported HIV prevalence [31] and reported morbid obesity prevalence [32,33], corrected for multiple conditions. The population of pregnant women is derived using the CDC's method combining fertility, abortion and fetal loss rates [39–41].

Table A4. High-risk conditions for influenza and data sources for prevalence estimation

Condition	Data source
Cancer (except skin), chronic kidney disease, COPD, coronary heart disease, stroke, asthma, diabetes	CDC 500 cities [28]
HIV/AIDS	CDC HIV Surveillance report [31]
Obesity	CDC 500 cities [28], Sturm and Hattori [32], Morgan et al. [33]
Pregnancy	National Vital Statistics Reports [39] and abortion data [40]

Table A5. Comparison between published national estimates and Austin-Round Rock MSA estimates of the percent of the population at high-risk of influenza/COVID-19 complications.

Age Group	National estimates [37]	Austin-Round Rock (excluding pregnancy)	Pregnant women (proportion of age group)
0 to 6 months	NA	8.1	-
6 months to 4 years	6.8	9.0	-
5 to 9 years	11.7	14.6	-
10 to 14 years	11.7	16.7	-
15 to 19 years	11.8	17.0	3.2
20 to 24 years	12.4	13.2	10.6
25 to 34 years	15.7	17.4	9.6
35 to 39 years	15.7	22.1	3.7
40 to 44 years	15.7	22.5	0.6
45 to 49 years	15.7	22.7	-
50 to 54 years	30.6	37.5	-
55 to 60 years	30.6	37.4	-
60 to 64 years	30.6	37.3	-
65 to 69 years	47.0	53.2	-
70 to 74 years	47.0	53.2	-
75 years and older	47.0	53.2	-

References

1. Sheikh A, McMenamin J, Taylor B, Robertson C, Public Health Scotland and the EAVE II Collaborators. SARS-CoV-2 Delta VOC in Scotland: demographics, risk of hospital admission, and vaccine effectiveness. Lancet. 2021;397: 2461–2462.

2. [No title]. [cited 7 Jul 2021]. Available: https://khub.net/documents/135939561/405676950/Increased+Household+Transmission+of+COVID-19+Cases+-+national+case+study.pdf/7f7764fb-ecb0-da31-77b3-b1a8ef7be9aa

3. Texas Department of State Health Services. Texas COVID-19 Data. [cited 15 Jul 2021]. Available: https://dshs.texas.gov/coronavirus/AdditionalData.aspx

4. Mitze T, Kosfeld R, Rode J, Wälde K. Face masks considerably reduce COVID-19 cases in Germany. Proc Natl Acad Sci U S A. 2020;117: 32293–32301.

5. Ionides EL, Nguyen D, Atchadé Y, Stoev S, King AA. Inference for dynamic and latent variable models via iterated, perturbed Bayes maps. Proc Natl Acad Sci U S A. 2015;112: 719–724.

6. Gao S, Rao J, Kang Y, Liang Y, Kruse J. Mapping county-level mobility pattern changes in the United States in response to COVID-19. arXiv [physics.soc-ph]. 2020. Available: http://arxiv.org/abs/2004.04544

7. Prem K, Cook AR, Jit M. Projecting social contact matrices in 152 countries using contact surveys and demographic data. PLoS Comput Biol. 2017;13: e1005697.

8. Verity R, Okell LC, Dorigatti I, Winskill P, Whittaker C, Imai N, et al. Estimates of the severity of COVID-19 disease. Epidemiology. medRxiv; 2020. doi:10.1101/2020.03.09.20033357

9. Baden LR, El Sahly HM, Essink B, Kotloff K, Frey S, Novak R, et al. Efficacy and Safety of the mRNA-1273 SARS-CoV-2 Vaccine. N Engl J Med. 2021;384: 403–416.

10. CDC. COVID Data Tracker. 28 Mar 2020 [cited 15 Jul 2021]. Available: https://covid.cdc.gov/covid-data-tracker/

11. e Conhecimento R de I. GISAID Initiative. 2021. Available: http://gisaid.org/

12. Austin Dashboard. [cited 16 Jul 2021]. Available: https://covid-19.tacc.utexas.edu/dashboards/austin/

13. Keeling MJ, Rohani P. Modeling Infectious Diseases in Humans and Animals. Princeton University Press; 2011.

14. Gillespie DT. Approximate accelerated stochastic simulation of chemically reacting systems. J Chem Phys. 2001;115: 1716–1733.

15. Johnson KE, Woody S, Lachmann M, Fox SJ, Klima J, Hines TS, et al. Early estimates of SARS-CoV-2 B.1.1.7 variant emergence in a university setting. medRxiv. 2021; 2021.03.05.21252541.

16. Liu Y, Gayle AA, Wilder-Smith A, Rocklöv J. The reproductive number of COVID-19 is higher compared to SARS coronavirus. J Travel Med. 2020;27. doi:10.1093/jtm/taaa021

17. R Core Team. R: A Language and Environment for Statistical Computing. Vienna, Austria: R Foundation for Statistical Computing; 2020. Available: https://www.R-project.org/

18. King AA, Nguyen D, Ionides EL. Statistical Inference for Partially Observed Markov Processes via the R Package pomp. arXiv [stat.ME]. 2015. Available: http://arxiv.org/abs/1509.00503

19. He X, Lau EHY, Wu P, Deng X, Wang J, Hao X, et al. Temporal dynamics in viral shedding and transmissibility of COVID-19. Nat Med. 2020. doi:10.1038/s41591-020-0869-5

20. Fox SJ, Pasco R, Tec M, Du Z, Lachmann M, Scott J, et al. The impact of asymptomatic COVID-19 infections on future pandemic waves. medRxiv. 2020. Available: https://www.medrxiv.org/content/10.1101/2020.06.22.20137489v1.abstract

21. Bernal JL, Andrews N, Gower C, Gallagher E, Simmons R, Thelwall S, et al. Effectiveness of COVID-19 vaccines against the B.1.617.2 variant. bioRxiv. medRxiv; 2021. doi:10.1101/2021.05.22.21257658

22. Zhang J, Litvinova M, Wang W, Wang Y, Deng X, Chen X, et al. Evolving epidemiology and transmission dynamics of coronavirus disease 2019 outside Hubei province, China: a descriptive and modelling study. Lancet Infect Dis. 2020. doi:10.1016/S1473-3099(20)30230-9

23. He D, Zhao S, Lin Q, Zhuang Z, Cao P, Wang MH, et al. The relative transmissibility of asymptomatic COVID-19 infections among close contacts. Int J Infect Dis. 2020;94: 145–147.

24. CDC. People at High Risk of Flu. In: Centers for Disease Control and Prevention [Internet]. 1 Nov 2019 [cited 26 Mar 2020]. Available: https://www.cdc.gov/flu/highrisk/index.htm

25. CDC - BRFSS. 5 Nov 2019 [cited 26 Mar 2020]. Available: https://www.cdc.gov/brfss/index.html

26. Zhang X, Holt JB, Lu H, Wheaton AG, Ford ES, Greenlund KJ, et al. Multilevel regression and poststratification for small-area estimation of population health outcomes: a case study of chronic obstructive pulmonary disease prevalence using the behavioral risk factor surveillance system. Am J Epidemiol. 2014;179: 1025–1033.

27. Tindale L, Coombe M, Stockdale JE, Garlock E, Lau WYV, Saraswat M, et al. Transmission interval estimates suggest pre-symptomatic spread of COVID-19. Epidemiology. medRxiv; 2020. doi:10.1101/2020.03.03.20029983

28. 500 Cities Project: Local data for better health | Home page | CDC. 5 Dec 2019 [cited 19 Mar 2020]. Available: https://www.cdc.gov/500cities/index.htm

29. Health Outcomes | 500 Cities. 25 Apr 2019 [cited 28 Mar 2020]. Available: https://www.cdc.gov/500cities/definitions/health-outcomes.htm

30. Part One: Who Lives with Chronic Conditions. In: Pew Research Center: Internet, Science & Tech [Internet]. 26 Nov 2013 [cited 23 Nov 2019]. Available:

https://www.pewresearch.org/internet/2013/11/26/part-one-who-lives-with-chronic-conditions/

31. for Disease Control C, Prevention, Others. HIV surveillance report. 2016; 28. URL: http://www cdc gov/hiv/library/reports/hiv-surveil-lance html Published November. 2017.

32. Sturm R, Hattori A. Morbid obesity rates continue to rise rapidly in the United States. Int J Obes . 2013;37: 889–891.

33. Morgan OW, Bramley A, Fowlkes A, Freedman DS, Taylor TH, Gargiullo P, et al. Morbid obesity as a risk factor for hospitalization and death due to 2009 pandemic influenza A(H1N1) disease. PLoS One. 2010;5: e9694.

34. Estimating the Number of Pregnant Women in a Geographic Area from CDC Division of Reproductive Health. Available: https://www.cdc.gov/reproductivehealth/emergency/pdfs/PregnacyEstimatoBrochure508.pdf

35. Miller GF, Coffield E, Leroy Z, Wallin R. Prevalence and Costs of Five Chronic Conditions in Children. J Sch Nurs. 2016;32: 357–364.

36. Cancer Facts & Figures 2014. [cited 30 Mar 2020]. Available: https://www.cancer.org/research/cancer-facts-statistics/all-cancer-facts-figures/cancer-facts-figures-2014.html

37. Hales CM, Fryar CD, Carroll MD, Freedman DS, Ogden CL. Trends in Obesity and Severe Obesity Prevalence in US Youth and Adults by Sex and Age, 2007-2008 to 2015-2016. JAMA. 2018;319: 1723–1725.

38. Zimmerman RK, Lauderdale DS, Tan SM, Wagener DK. Prevalence of high-risk indications for influenza vaccine varies by age, race, and income. Vaccine. 2010;28: 6470–6477.

39. Martin JA, Hamilton BE, Osterman MJK, Driscoll AK, Drake P. Births: Final Data for 2017. Natl Vital Stat Rep. 2018;67: 1–50.

40. Jatlaoui TC, Boutot ME, Mandel MG, Whiteman MK, Ti A, Petersen E, et al. Abortion Surveillance - United States, 2015. MMWR Surveill Summ. 2018;67: 1–45.

41. Ventura SJ, Curtin SC, Abma JC, Henshaw SK. Estimated pregnancy rates and rates of pregnancy outcomes for the United States, 1990-2008. Natl Vital Stat Rep. 2012;60: 1–21.